



### Influence of Dityrosine Nanotubes on the Expression of Dopamine and Differentiation in Neural Cells

Journal:	<i>Journal of Materials Chemistry B</i>
Manuscript ID	TB-ART-11-2020-002680.R2
Article Type:	Paper
Date Submitted by the Author:	06-Apr-2021
Complete List of Authors:	<p>Macha, Prathyushakrishna; University of Massachusetts Dartmouth, Bioengineering            Mayes, Maricris; University of Massachusetts Dartmouth College of Arts and Sciences, Chemistry and Biochemistry            Visayas, Benjoe Rey; University of Massachusetts Dartmouth College of Arts and Sciences, Chemistry and Biochemistry            Soni, Vikas; University of Massachusetts Dartmouth College of Engineering, Bioengineering; The George Washington University, Mechanical Engineering            Sammeta, Vamshikrishna Reddy ; University of Massachusetts Dartmouth, Chemistry and Biochemistry            Vasudev, Milana; University of Massachusetts Dartmouth, Bioengineering</p>

## Influence of Dityrosine Nanotubes on the Expression of Dopamine and Differentiation in Neural Cells

Received 9th July 20xx,  
Accepted 00th January 20xx

Prathyushakrishna Macha,<sup>a</sup> Maricris L. Mayes,<sup>b</sup> Benjoe R. B. Visayas,<sup>b</sup> Vikas Soni,<sup>a,c</sup> Vamshikrishna Reddy Sammeta,<sup>b</sup> and Milana C. Vasudev<sup>a,\*</sup>

DOI: 10.1039/x0xx00000x

In this study, we report the synthesis of self-assembled dityrosine nanotubes as a biologically functional scaffold and their interactions with neural cells. Quantum chemical methods were used to determine the forces involved in the self-assembly process. The physicochemical properties of the nanostructures relevant to their potential as bioactive scaffolds were characterized. The morphology, secondary structure, crystallinity, mechanical properties, and thermal characteristics of the YY nanotubes were analyzed. The influence of these nanotubes as scaffolds for neural cells were studied *in vitro* to understand their effects on cell proliferation, morphology, and gene expression. The scanning electron and fluorescence confocal microscopy demonstrated the feasibility of nanotube scaffolds for enhanced adhesion to rat and human neural cells (PC12 and SH-SY5Y). Preliminary ELISA and qPCR analysis demonstrated the upregulation in dopamine synthesis and gene involved in the dopamine expression and differentiation. The expression levels for D $\beta$ H, AADC, VMAT2 and MAOA in SH-SY5Y cells cultured on the nanotube scaffolds for 7 days were elevated in comparison to the control cells.

**Introduction.** Self-assembled peptide nanomaterials for tissue engineering and regenerative medicine has garnered increasing interest in the past decade. Peptide-based nanomaterials are attractive due to their chemical versatility, biological recognition capabilities and biodegradability.<sup>1-3</sup> Dityrosine (YY) is a dipeptide motif that is commonly found in protein cross-links and plays a crucial role in stabilizing proteins such as elastin, variety of silks, and wheat gluten.<sup>4-6</sup> Such crosslinks are also frequently present in areas prone to high stress in mammalian structural and connective tissues due to their role in the stability and providing strength. These crosslinks are further implicated in the formation of insoluble aggregates of  $\beta$ -sheet rich fibrils in intrinsically disordered proteins such as  $\alpha$ -synuclein. However, from a biomaterials perspective, the role of self-assembled dityrosine nanomaterials needs to be probed.<sup>7, 8</sup> Dityrosine cross-links have been utilized recently, in the design of biopolymers but YY has itself not been probed for its ability to self-assemble into nanostructures under suitable conditions.<sup>9-11</sup>

Tyrosine with its phenolic side groups, and chemical reactivity, facilitates molecular interactions and high redox potentials. Tyrosine can undergo transient oxidation and reduction due to the deprotonation of the oxygen in the phenol ring and the

formation of tyrosyl radicals due to deprotonation, is useful in controlling the kinetics and thermodynamics of electron transfer under physiological conditions.<sup>12, 13</sup> Tyrosine is a precursor in the dopamine (DA) synthesis and metabolism pathway with the involvement of enzymes such as tyrosine hydroxylase (TH) and aromatic amino acid decarboxylase (AADC). Dopaminergic neurons involved in stress response, working memory and cognitive function regulation are affected by tyrosine levels in the brain. Prior studies reported that the cognitive functions in the brain mediated by DA were affected by varying tyrosine levels. Numerous pharmacological approaches have been used to modulate the release of neurotransmitters such as DA, epinephrine, and norepinephrine.<sup>14-18</sup> Supplementation with L-tyrosine, did not interfere with the endogenous pool but was converted to DA. Serotonin and DA metabolisms improved in individuals with phenylketonuria following the administration of tyrosine tablets.<sup>15</sup> The precursor availability has an ability to influence the synthesis of neurotransmitters such as DA. The converging data from several animal and human studies suggest that the DA synthesis and metabolism is influenced by tyrosine availability.

In this study, we have investigated the intermolecular interactions involved in YY-based nanostructure formation, synthesis of YY nanotubes, stability in physiological conditions and their effect on neural cell differentiation and DA release. Self-assembly of aromatic dipeptides involves complex non-covalent interactions, and understanding these forces allows manipulation of material properties at a molecular scale. Due to tremendous improvements in computer performance and advances in method development, computational techniques have become an essential approach to study this complex

<sup>a</sup> Department of Bioengineering, University of Massachusetts Dartmouth, Dartmouth, MA 02747, USA

<sup>b</sup> Department of Chemistry and Biochemistry, University of Massachusetts Dartmouth, Dartmouth, MA 02747, USA

<sup>c</sup> Department of Mechanical Engineering, George Washington University, DC 20052, USA

E-mail: [mvasudev@umassd.edu](mailto:mvasudev@umassd.edu)

Electronic Supplementary Information (ESI) available: [details of any supplementary information available should be included here]. See DOI: 10.1039/x0xx00000x

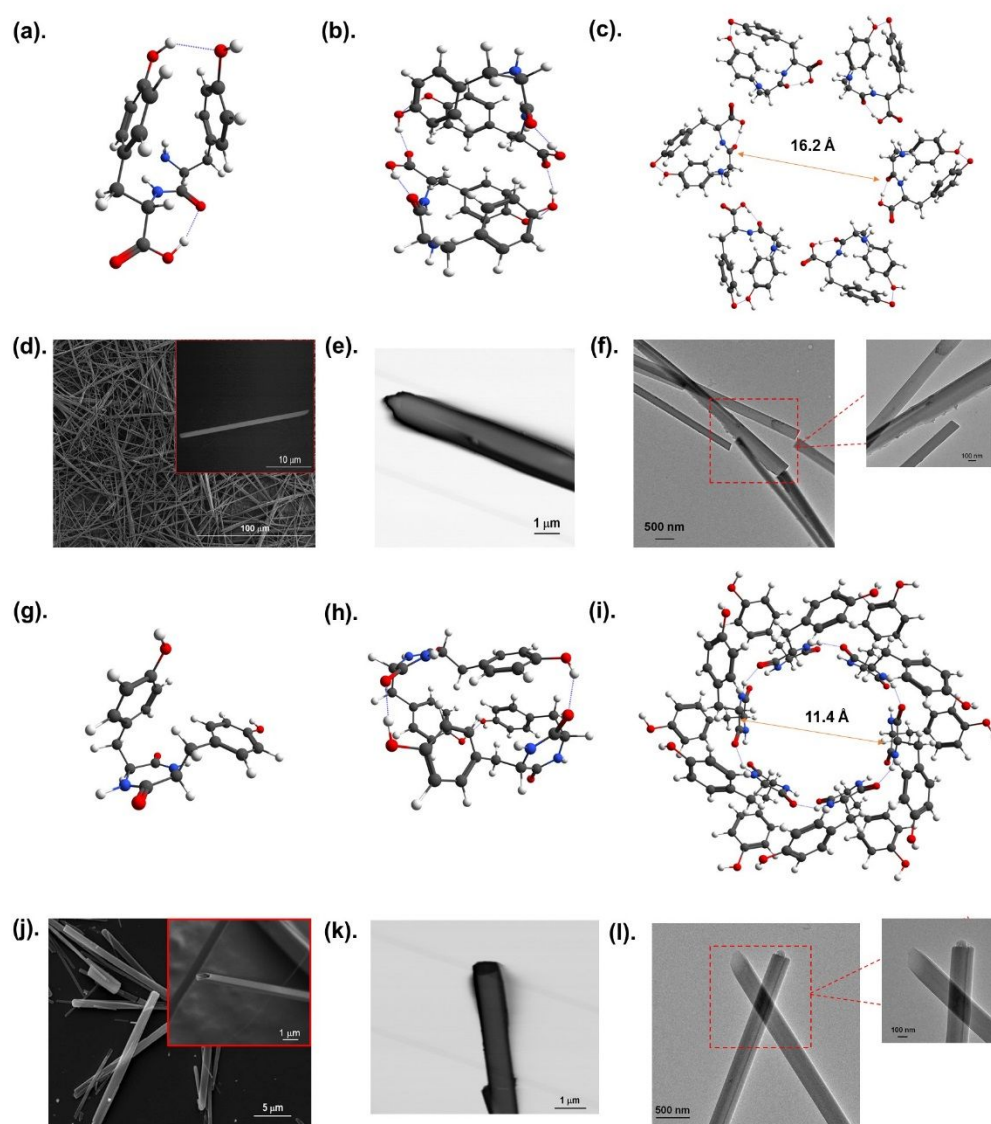


**Figure 1.** Calculated structures of the most stable conformer (a). Linear YY monomer (b). Linear YY dimer (c). Linear YY hexamer; Electron microscopy images of linear YY nanotubes (d). SEM (inset: higher magnification), (e). STEM C image (f). High magnification TEM images; Calculated structures of the most stable conformer (g). Cyclic YY monomer, (h). Cyclic YY dimer, (i). Cyclic YY hexamer; and electron microscopy images of cyclic YY nanotubes (j). SEM (inset: higher magnification image of open nanotubes), (k). STEM image, (l). TEM high magnification images.

problem. Electronic structure studies of non-covalent interactions highlight the need for an accurate description of dispersion. The pair interaction energy decomposition analysis was used to analyze the interaction between YY molecules, and the total interaction energy is decomposed into electrostatic, exchange-repulsion, charge-transfer, and dispersion contributions. We have employed quantum chemical computational methods to study the lowest possible energy conformations of the monomeric, dimeric, and hexameric forms of YY and to probe the interactions, driving forces, and thermodynamics involved in the initial aggregation. The cyclic

YY nanotubes were used as a scaffold that could provide the topographical cues required for differentiation. The applications of linear aromatic peptide nanostructures have been limited due to issues associated with their stability at physiological pH. Heat-induced cyclization lead to the formation of physiologically stable nanotubes, removal of the solvents involved in the self-assembly process and may avoid the complexities associated with the synthesis of cyclic peptides.<sup>19</sup> *In vitro* studies were carried out to understand the effects of the YY nanotubes on the morphology, differentiation, DA expression and associated gene expression changes in two

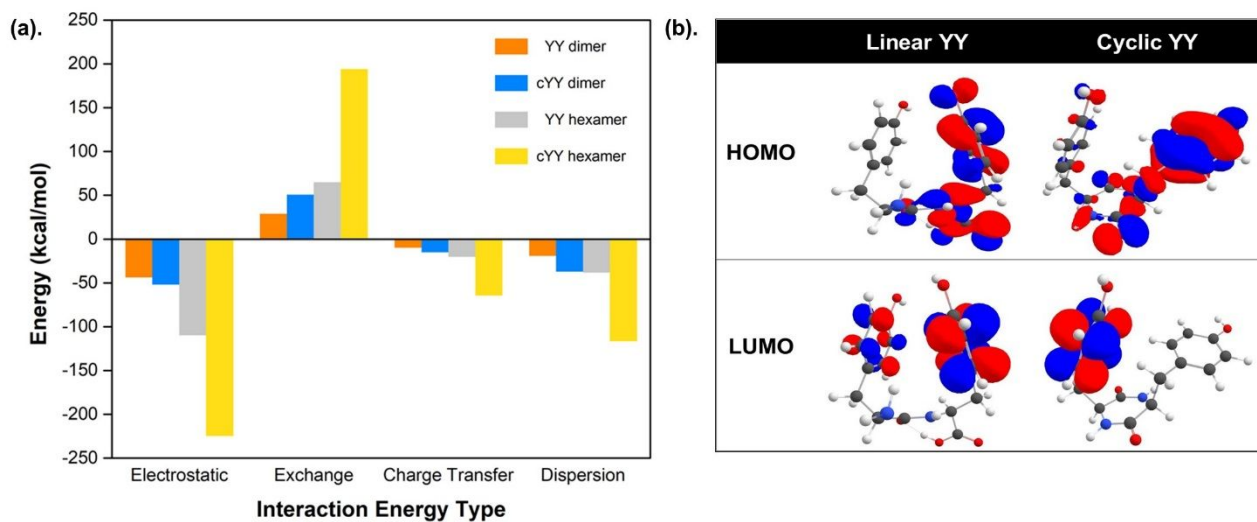


**Figure 2.** (a). Interaction energy in the linear and cyclic YY dimers and hexamers; (b). Highest-occupied molecular orbital (HOMO) and

*lowest-unoccupied molecular orbitals (LUMO) of the lowest energy conformer of linear YY and cyclic YY monomers.*

different neural cell lines, PC12, and SH-SY5Y cells. PC12 is a model cell-line from the rat pheochromocytoma used for neural differentiation, gene expression, neurotoxicity, and DA release studies.<sup>20, 21</sup> SH-SY5Y is a human neuroblastoma cell-line that has many characteristics of dopaminergic neurons and expresses biomarkers for DA release and can differentiate into mature and functional neural phenotype.<sup>22, 23</sup> The changes in gene expression associated with the genes involved in the process of differentiation and DA release were studied utilizing quantitative polymerase chain reactions (qPCR).<sup>24, 25</sup> The specific markers studied in SH-SY5Y cells were pertaining to DA synthesis and release. Aromatic L-amino acid decarboxylase (AADC) is important for the decarboxylation in the catecholamine (DA) synthesis.<sup>26</sup> Monoamine oxidase A (MAOA), and catechol-O-methyltransferase (COMT) play an important role in the metabolism of DA into inactive metabolites.<sup>27, 28</sup> Vesicular monoamine transporter-2 (VMAT2) is the synaptic vesicular transporter of DA, plays an important role in normal neurotransmission to maintain the intracellular levels of DA and avoids neuronal damage.<sup>29, 30</sup> Dopamine beta hydroxylase (DBH) catalyzes the conversion of dopamine and norepinephrine. In PC12 cells, COMT and Beta III-Tubulin was analyzed.<sup>21</sup> The interaction of the cyclic YY nanotubes with cellular dendrites could trigger the cellular differentiation pathway, causing the upregulation of genes involved in differentiation such as  $\beta$ -III tubulin. Nanoscale topographies such as pores, ridges, fibers and other 3D features provide cues for cellular growth and proliferation. The influence of 3D topographical features on the cellular responses in vivo is not very well understood.<sup>31, 32</sup> Cyclic YY nanotubes used in this study could potentially provide the topographical cues required for differentiation. The two major indicators studied were (i) morphological changes in the cells, and (ii) regulation of genes for signaling molecules or neurotransmitters such as DA. Since neural cells cannot repair or heal after being damaged either due to brain injury, trauma, or degenerative disorders, it is beneficial to study the interaction between nanotube scaffold

and cells since these nanotubes behave as bioactive scaffolds promoting neural proliferation and differentiation.

## B. Materials and Methods.

**Computational Methods.** The lowest energy conformers of linear YY and cyclic YY monomers and dimers, and their corresponding IR spectra, were determined using density functional theory (DFT) using M05<sup>33</sup> functional and 6-31G\*<sup>34</sup> basis set using GAMESS<sup>35</sup> program. The Grimme's dispersion corrections were used.<sup>36</sup> For the larger systems, such as the hexamers of YY, the dispersion-corrected third-order density functional-based tight-binding method (DFTB3-D) was used, employing the 3OB parameter set which is specifically designed for organic and biological systems.<sup>37, 38</sup> The latter method was used due to reduced computational cost compared to standard DFT methods. The hexamers were constructed from the optimized structures of the single dipeptide (monomer). The initial cyclic hexamer structures were built utilizing the central dipeptide ring as the inner nanotube wall placing the rings side-by-side to establish intermolecular hydrogen bonds between

adjacent C=O and N-H bonds of adjacent monomers. For the linear YY hexamer, the inner nanotube wall comprises the dipeptide backbone placing the C-terminus near the N-terminus. The pair interaction energy decomposition analysis (PIEDA)<sup>36</sup> using fragment molecular orbital (FMO)<sup>39</sup> method at the second order Møller–Plesset perturbation theory (FMO-MP2) and natural bond orbital (NBO)<sup>40</sup> analysis was used to investigate the nature of the interactions present in more detail. To study the effect of solvent, the solvation model based on density (SMD)<sup>41</sup> was used, using acetone as the solvent because it has a comparable dielectric constant to hexafluoroisopropanol used in the experiment. The UV-Vis and CD spectra were calculated using time-dependent (TD) DFT (SI Figure 3). The initial structures from DFTB3-D were optimized (with loose convergence) at M06-D3/6-31G\*<sup>34</sup> in ORCA<sup>42</sup> and then TDDFT ( $n_{\text{root}} = 1000$ ) was done on each geometry employing the sTDDFT mode.

**Synthesis of nanotubes.** Linear YY (H-Tyr-Tyr-OH), was purchased from Bachem (Switzerland). To form nanotubes, linear dipeptide was dissolved at a high concentration, (100 mg/mL) in an acidified solution of 1,1,1, 3,3,3-hexafluoro-2-propanol (HFIP 99%, Sigma) containing 10  $\mu$ L of 0.1 M hydrochloric acid (HCl) followed by dilution in water (1 mL) and overnight incubation at 4 °C. The nanotubes were lyophilized and subjected to heat treatment both in a vacuum and microwave oven, at their glass-liquid transition temperatures, which lead to their cyclization.

**Morphological characterization.** Scanning electron microscope (Hitachi SU-5000) with an accelerating voltage range of 0.5 kV to 2 kV was used in the morphological characterization of the synthesized nanotubes. The diluted nanotubes were deposited on clean aminosilane treated silicon wafer and air-dried at room temperature for SEM imaging. Samples were then sputter coated with 4 nm gold before imaging. Scanning transmission electron micrographs of the nanotubes were obtained using Hitachi SU-5000 with a STEM detector (Deben), and an accelerating voltage of 30 kV. Nanotubes were diluted from 1 mg/mL to 100  $\mu$ g/mL in water and 5  $\mu$ L was deposited onto formvar/carbon-coated grids and dried. High resolution transmission electron micrographs of the nanotubes were imaged at 100 KV using the Phillips CM200. The Zeiss 710 (Carl Zeiss, Thornwood, NY, USA) confocal microscope was used for imaging the cellular interactions of the nanotubes (stained with phalloidin-rhodamine,  $\beta$  III-tubulin, and nuclear stain, Hoechst).

**Infrared and Raman spectroscopy.** Infrared (FTIR) and Raman spectroscopy were used to study the self-assembly on the various dipeptides. Digilab Excalibur Fourier transform spectrometer 3000 was used for the FTIR measurements. Finely divided samples were combined with crystalline potassium bromide (KBr) to form a pellet. Spectra were obtained at an average of 100 scans (resolution of 2  $\text{cm}^{-1}$ ), with a range of 400  $\text{cm}^{-1}$  to 3600  $\text{cm}^{-1}$  and speed of 2.5 kHz. Raman spectra were collected using WITec's alpha 300 M confocal Raman system.

Averaged spectra from five acquisitions and 4 sec integration time were obtained.

**CD spectroscopy.** Circular dichroism analysis of linear YY peptide, and cyclized YY nanotubes was performed on a J-810 (Jasco, Inc. Tokyo, Japan) spectropolarimeter averaged over three scans with a range of 190 – 300 nm, and speed of 20 nm/min. Stock solutions of the nanotubes were diluted in double distilled water to final concentrations of 0.025 mg/mL, 0.8 mg/mL, and 0.125 mg/mL, respectively. Spectral data was processed using the CDSSTR, CONTIN-LL, and SELCON3 methods available in Dichroweb.

**NMR Spectroscopy.** The lyophilized linear peptide and cyclized nanotube samples were dissolved at a concentration of 10 mg/mL in deuterated DMSO and loaded in Bruker AVANCE III HD 400 MHz High-Performance Digital NMR for their respective <sup>1</sup>H and <sup>13</sup>C NMR spectra. The chemical shifts were analyzed using the MestReNova package and structures were drawn in ChemDraw.

**Nanoindentation.** The Agilent Nanoindenter XP MTS instrument with a continuous stiffness measurement (CSM) option was used to obtain the bulk Young's modulus of the peptide nanotubes on a silicon substrate. The contact force was measured with a cylindrical flat-punch indenter (40 μm tip).

**Cell culture.** Rat pheochromocytoma cells (PC12), and human neuroblastoma cells (SH-SY5Y), were obtained from the American Type Culture Collection (ATCC) and maintained at 37 °C with 95% humidity and 5% CO<sub>2</sub>.<sup>20</sup> PC12 cells were grown in RPMI 1640 media supplemented with 5% fetal bovine serum and 10% horse serum. SH-SY5Y Cells were cultured in 1:1 EMEM: F-12 supplemented with 5% fetal bovine serum.<sup>22, 43</sup> Cyclized YY nanotubes at concentrations of 2–4 mg/mL were deposited on glass coverslips (5 mm diameter) treated with aminosilane (5% in methanol). The coverslips were seeded with cells (5 × 10<sup>3</sup> cells/coverslip) and cultured in 96-well plates for the cell viability assay. Media changes were performed within the first 12–24 hours to remove any unattached cells. The cell viability and growth were recorded on days 3, and 5 using the methyl tetrazolium (MTT) reagent at a final concentration of 0.5 mg/mL.<sup>44</sup> Absorbance measurements were carried out at 570 nm using a Multiskan™ FC microplate reader (Thermo Scientific™). Cells on nanotubes were fixed at 72 hours using 2.5% glutaraldehyde (primary fixative) and 1% osmium tetroxide (secondary fixative) in dH<sub>2</sub>O. Following fixative, samples were washed with phosphate-buffered saline (PBS) and further dried using hexamethyldisilazane (HMDS) as a chemical alternative to critical point drying.

**RNA Extraction.** RNeasy kit from Qiagen was used to extract and purify high-quality ribonucleic acid (RNA) from PC12 cells cultured on nanotubes for 8 days. RNA was suspended in RNase-free water at 100–300 ng concentration for complementary deoxyribonucleic acid (cDNA) preparation. The Bio-Rad iScript cDNA kit was used to synthesize cDNA from the purified RNA and cDNA was diluted to a concentration of ~100 ng/μL for qPCR measurements. The cDNA was diluted in 1:1 volume of

nuclease-free water and absorbance was measured using a nanodrop.

**qPCR.** The specific markers studied in the case of SH-SY5Y cells were pertaining to DA synthesis and release. Aromatic L-amino acid decarboxylase (AADC) is important for the decarboxylation in the catecholamine (DA) synthesis. Monoamine oxidase A (MAOA), and catechol-O-methyltransferase (COMT) play an important role in the metabolism of DA into inactive metabolites. COMT activity also plays a role in the regulation of active DA in the brain.<sup>27</sup> Vesicular monoamine transporter-2 (VMAT2) is a synaptic vesicular transporter of DA, and plays an important role in maintaining the intracellular levels of DA and avoids neuronal damage. Dopamine beta hydroxylase (DβH) catalyzes the conversion of DA and norepinephrine.<sup>29</sup> Class III β-tubulin, (β III-tubulin) is a part of the tubulin family and found in neurons.<sup>45</sup> RNA polymerase II (RP II) and glyceraldehyde 3-phosphate dehydrogenase (GAPDH) were used as internal standards. The specific primers used are listed in Tables S1 and S2 of supporting information.

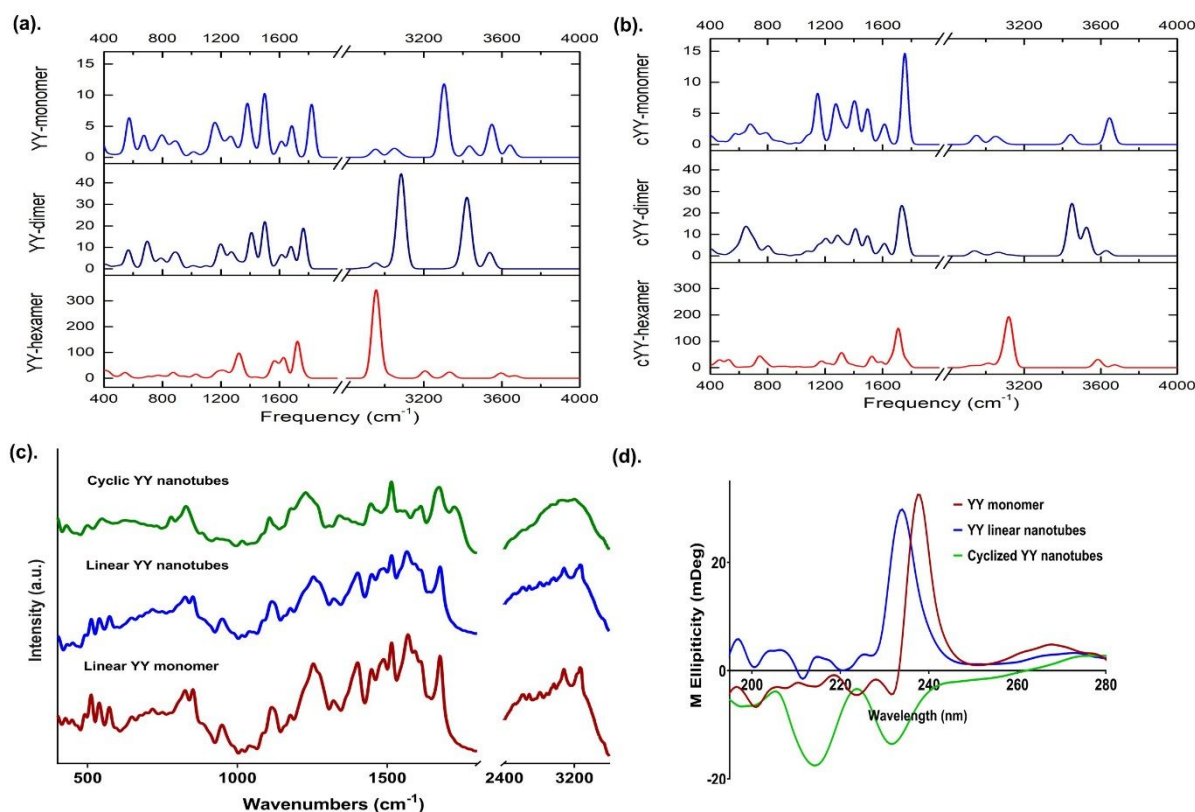


**Figure 3.** Calculated IR spectra of (a). Linear YY and (b). Cyclic YY; (c). FTIR spectra of linear YY and cyclic YY nanotubes; (d). CD spectral analysis of the linear and cyclic YY nanotubes.

The Bio-Rad SYBR green mix was used for a total reaction volume of 10  $\mu\text{L}$ /well. The reaction mix contained SYBR green mix (5  $\mu\text{L}$ /well), forward and reverse primers of corresponding biomarkers (2  $\mu\text{L}$ /well), template DNA (cDNA diluted, 1  $\mu\text{L}$ /well) and RNase-free water for the rest of the volume. The Roche Lightcycler 480 was used for qPCR analysis. The standard curve was calculated using the cDNA of different concentrations ranging from 4X, 8X, 16X & 64X, respectively. We have validated the qPCR results using the  $\Delta\Delta\text{Ct}$  method.<sup>46</sup> The PCR cycle number at which fluorescence emission reaches a threshold above the baseline emission determines the cycle threshold (Ct). The Ct value for each gene tested was normalized with the Ct value of housekeeping genes (GAPDH and RPII).<sup>47</sup>

**ELISA.** PC12 and SH-SY5Y cells were seeded at a density of 2000 cells/mm on a 10 mm, glass coverslip coated with YY nanotubes for 7 days in a 12-well plate. The media from each well corresponding to the cyclized nanotubes was combined with the cell lysates of each well to capture both inter- and intracellularly released DA. The extraction process followed by a colorimetric competitive enzyme linked immunosorbent assay (ELISA) with an absorbance of 450 nm was performed in accordance with the kit from Rocky Mountain Diagnostics, Inc. (Catalog #BA E-5300). The samples were measured in triplicates at 1:5 and 1:10 dilutions. The average values of the 1:10 dilutions were found to be within the range of the standard curve (0, 0.5, 1.5, 5, 20, 80 ng/mL) and the DA concentrations in

the samples were calculated based on the defined DA concentrations of the standard curve.<sup>48, 49</sup>

### C. Results and discussion

The conformational and vibrational analysis of the isolated linear and cyclic forms of YY, which we refer to as monomers here, showed that the most stable conformer for linear YY was characterized by hydrogen bonding of the carboxylic hydroxyl group with the carbonyl of the amide as shown in our previous work (**Figure 1a**).<sup>19, 50</sup> The lowest energy noncovalent dimer of linear YY is characterized by two intermolecular hydrogen bonding of the carboxylic group of one dipeptide with the tyrosine hydroxyl group of the other dipeptide

( $O_{\text{carboxyl}} \cdots H(O)_{\text{tyr}}$ ), within 1.94 Å (**Figure 1b**). The optimized structure for the lowest conformer of noncovalent hexamer of linear YY has its C-terminal hydrogen-bonded internally with the monomer's amide bond. This structure has 12 intramolecular hydrogen bonds and six intermolecular  $O_{\text{carboxyl}} \cdots H_2N$  with an average length of 2.11 Å. It has an inner diameter of 16.2 Å measured between two opposite monomers' carbonyl carbons (**Figure 1c**).

On the other hand, for cyclic YY monomer, the most stable conformer has a slightly puckered boat structure for the diketopiperazine ring with the aromatic side chains in pseudoaxial and pseudo-equatorial positions (**Figure 1g**). The lowest energy noncovalent dimer of cyclic YY exhibited two intermolecular hydrogen bonding between a peptide carbonyl

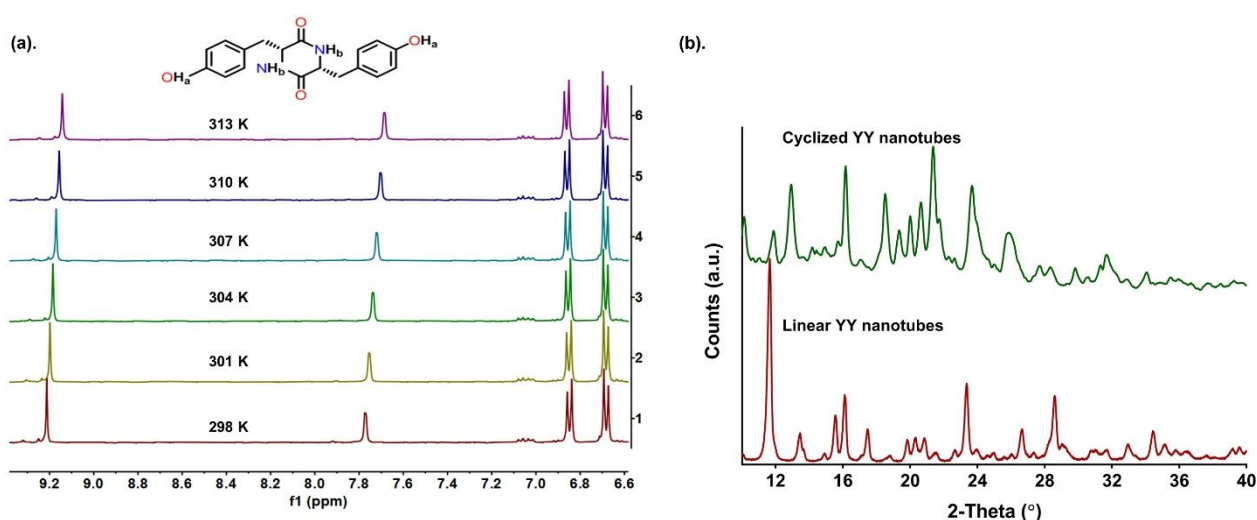


**Figure 4.** (a). Temperature dependent NMR spectroscopy indicating the formation of nanotubes with increasing temperatures from 298 K–313 K in deuterated DMSO; (b). XRD analysis of linear and cyclized YY nanotubes.

group and a tyrosine hydroxyl group of the opposite monomer ( $O_{\text{carboxyl}} \cdots H(O)_{\text{tyr}}$ ) within 1.87 Å, one hydrogen bonding between tyrosine hydroxyl groups ( $H(O)_{\text{tyr}} \cdots H(O)_{\text{tyr}}$ ), and  $\pi_{\text{tyr}} \cdots C(H)$  within 2.50 Å (**Figure 1h**). The lowest optimized structure for the noncovalent hexamer of cyclic YY has asymmetric conformation of the lowest energy monomers positioned side-by-side while maintaining the pseudoaxial and pseudo-equatorial sidechain conformations. The inner diameter for this structure, measured between the centers of amide rings of opposite monomers is 11.4 Å. The cyclic YY hexamer has 12 intermolecular  $O_{\text{carboxyl}} \cdots H(N)_{\text{peptide}}$  with an average length of 1.82 Å on one end and 2.01 Å on the other (**Figure 1i**).

Electron microscopy imaging of the self-assembled linear YY nanotubes, (**Figure 1d and 1e**) indicate that the linear YY peptide formed nanostructures with high aspect ratios. In parallel, the self-assembled linear YY tubes (**Figure 1d**) were subjected to a glass-phase transition temperature of 267 °C. The

glass-transition temperature was determined using the differential scanning calorimetry (DSC) and thermogravimetric analysis (TGA) (**SI Figure S1**). This thermal treatment induces a phase transition into a cyclized form due to the loss of water molecule (18 g/mol) in the dipeptide assemblies and the formation of an additional amide bond (**Figure 1g**). Cyclization or loss of water molecule leads to the formation of a 2,5-diketopiperazine ring which contributes to improved interactions and stability (**Figure 1g**) and is verified using liquid chromatography combined with mass spectroscopy (**SI Figure S2**). The phase transition between linear and cyclic forms was confirmed on the chromatogram with the change in molecular weights from 345.06 g/mol  $\rightarrow$  327.06 g/mol following the heating at the glass-transition temperature for 15 mins. SEM and STEM imaging (**Figure 1j and 1k**) of heat-treated cyclized YY peptide were tubular and shorter in comparison to the linear YY nanotubes. Comparison of the STEM micrographs of linear and cyclized YY nanotubes indicate that linear nanotubes were flat and longer when compared to the cyclized nanotubes (**Figures**

**1e and 1k**). The change in aspect ratio leads to higher physical stability of these tubes, also observed in tryptophan-tyrosine nanotubes in our previous study.<sup>19</sup> The TEM micrographs of the linear and cyclized YY nanotubes show the structure of individual nanotubes and confirm the dimensions and hollow nature of the nanotubes (**Figure 1f and 1l**). Individual cyclized nanotubes appeared to have uniform diameter and were cylindrical in shape.

The cyclic forms of YY have higher total interaction energy than their linear form counterparts. The electrostatic and dispersion energy is dominant in cyclic YY dimer due to two intermolecular  $O_{\text{carboxyl}} \cdots H(O)_{\text{tyr}}$  hydrogen bonding,  $OH_{\text{tyr}} \cdots O(H)_{\text{tyr}}$ , and  $\pi_{\text{tyr}} \cdots C(H)$  interactions, which are all confirmed in NBO calculations (**Figure 2a**). In contrast, for linear form YY dimer, the contribution is mostly electrostatic due to two intermolecular  $O_{\text{carboxyl}} \cdots H(O)_{\text{tyr}}$  hydrogen bonding. The donor-acceptor stabilization energies in cyclic YY is stronger than linear YY. The same is true for the formation of hexamers. Electrostatic

interaction is dominant, confirming the importance of intermolecular and intramolecular hydrogen bonding, almost doubled for cyclic YY hexamer compared to linear YY hexamer. The results also show increased charge transfer, exchange, and dispersion for cyclic YY hexamer over linear YY hexamer. The results imply the importance of van der Waals interactions between partially charged termini and tyrosine aromatic rings on adjacent dipeptides and  $\pi \cdots \pi$  interaction. The Gibb's energy for the formation of cyclic YY dimer (-5.76 kcal/mol) is lower than linear YY dimer (-4.50 kcal/mol), as calculated by DFTB-D3. Using the same level of theory, the formation of linear YY hexamer is not spontaneous, however the formation of cyclic YY hexamer is spontaneous. This demonstrates that cyclization stabilizes the dipeptide and that cyclic YY hexamers are more likely to self-assemble than the linear ones. The highest-occupied molecular orbital (HOMO) and lowest-unoccupied molecular orbitals (LUMO) of the lowest energy conformer of linear YY and cyclic YY monomers are shown in **Figure 2b**. The HOMO consists of the  $\pi$ -orbitals of one of the tyrosine rings,

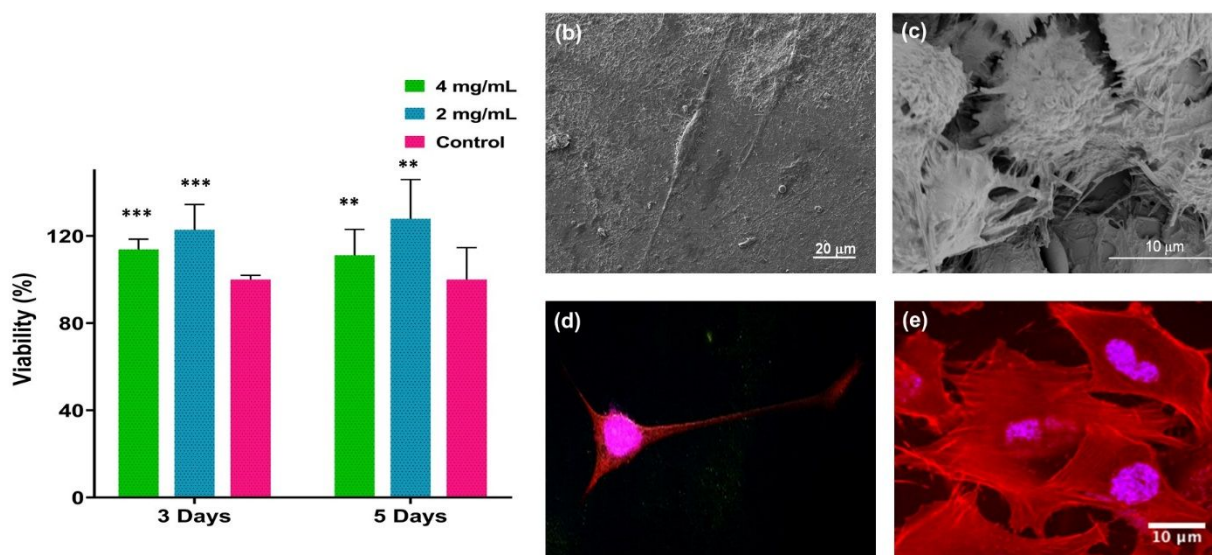


**Figure 5.** (a). Cell metabolic activity and viability assay (MTT) for PC12 cells grown on the cyclized YY nanotubes scaffold at 3- and 5 days post-seeding ( $*** P < 0.005$  and  $** P < 0.05$ ,  $n=3$ ) (b). SEM image of PC12 cells cultured on the cyclized YY nanotubes substrates; (c). SEM image of control PC12 cells; (d). Confocal imaging of PC12 cells stained with phalloidin-rhodamine and counterstained with DAPI on cyclized YY nanotubes scaffold (e). Confocal imaging of PC12 control cells seeded on glass coverslips.

whereas the LUMO contains the  $\pi^*$  orbitals of the other tyrosine ring for the cyclic YY. The difference in localization of electron density between the HOMO and LUMO demonstrates the importance of charge-transfer interactions in these systems. Computational calculated absorbance (UV-Vis) peaks are comparable to the experimental measurements (**SI Figure S3**).

Computational FTIR peaks for *linear YY monomer*, some of the representative peaks include free hydroxyl groups ( $OH_{\text{tyr}}$ ) on each of the phenolic rings of YY (3534 and 3621  $\text{cm}^{-1}$ ), peptide N—H stretching ( $NH_{\text{pep}}$ , 3377  $\text{cm}^{-1}$ ), the intense carboxyl O—H stretch ( $OH_{\text{carboxyl}}$ , 3231  $\text{cm}^{-1}$ ), the carbonyl of the carboxyl group ( $CO_{\text{carboxyl}}$ , 1756  $\text{cm}^{-1}$ ) and carbonyl peptide stretching

vibrations ( $CO_{\text{pep}}$ , 1641  $\text{cm}^{-1}$ ), the peptide N—H in-plane bending vibration ( $NH_{\text{ipb}}$ , 1490  $\text{cm}^{-1}$ ), and carboxyl O—H in-plane bending vibration ( $OH_{\text{ipb}}$ , 1256  $\text{cm}^{-1}$ ) (**Figure 3a**). The characteristic peaks that are present in the monomer are also present in the dimers. For the *linear YY dimer*, the  $OH_{\text{tyr}}$  occurs at 3537 and 3423  $\text{cm}^{-1}$ , the latter a red-shift of about 200  $\text{cm}^{-1}$  with respect to the monomer, which is a characteristic of intermolecular  $O_{\text{carboxyl}} \cdots H(O)_{\text{tyr}}$ . The intense  $OH_{\text{carboxyl}}$  peaks at around 3084  $\text{cm}^{-1}$ , also a red-shift of about 200  $\text{cm}^{-1}$ . For the *lowest linear YY hexamer*, the most prominent is the  $OH_{\text{carboxyl}}$  peak at around 3025  $\text{cm}^{-1}$  (**Figure 3a**). For *cyclic YY monomer*, the calculated IR spectrum shows  $OH_{\text{tyr}}$  at 3645 and 3646  $\text{cm}^{-1}$ ,  $NH_{\text{pep}}$  occurs at 3439 and 3449  $\text{cm}^{-1}$ , and  $CO_{\text{pep}}$  stretching vibrations appear at 1754 and 1760  $\text{cm}^{-1}$ . For *cyclic YY dimer*, the characteristic change is the  $O_{\text{carboxyl}} \cdots H(O)_{\text{tyr}}$ , which occur at 3435 and 3441  $\text{cm}^{-1}$ . For the *cyclic YY hexamer*, the inter- and intramolecular  $O_{\text{carboxyl}} \cdots HN$  peaks are very intense

and observed at around  $3100\text{ cm}^{-1}$  (**Figure 3b**). Experimental Fourier transform infrared spectra (FTIR) also indicates significant differences between linear and cyclized YY

nanotubes (**Figure 3c**). The Amide I peak due to the carbonyl (C=O) stretching of dipeptide backbone in the range of  $1600\text{--}1700\text{ cm}^{-1}$  with peaks at  $1678\text{ cm}^{-1}$  and  $1615, 1676\text{ cm}^{-1}$  for linear and cyclized YY nanotubes, respectively. A peak shift of  $40\text{ cm}^{-1}$  was observed in the  $1723\text{ cm}^{-1}$  peak. Another significant difference was noted in the N-H stretching, a broad single peak for cyclized YY nanotubes and a doublet for linear YY nanotubes was observed in the range of  $3100\text{--}3300\text{ cm}^{-1}$ , indicating the presence of a secondary amine group in the former and a primary amine group in the latter's assembly.<sup>51, 52</sup> Raman peaks of cyclized and linear nanotubes had some significant differences in the secondary conformation region with peaks at  $1621\text{ cm}^{-1}$  in the cyclized YY nanotubes (**SI Figure S4a**).<sup>53, 54</sup> A

small O-H stretch peak was observed in cyclized YY nanotubes at  $3230\text{ cm}^{-1}$  while a broader peak in the same range was observed in the case of linear YY nanotubes. Circular dichroism analysis was carried out to reveal the predominant secondary structural conformations in linear and cyclized YY nanotubes (**Figure 3d**). YY linear nanotubes with a CD peak at  $233\text{ nm}$ . Prior studies indicate that a strong positive peak around  $230\text{ nm}$  can be attributed to a  $\pi$ -cation interaction.<sup>55, 56</sup> However, in cyclized YY nanotubes, the cyclization process leads to a conformational composition of mainly  $\alpha$ -helices ( $\sim 50\%$   $\alpha$ -helices). The molar ellipticity calculations using TD-DFT concur with the experimental results (**SI Figure S4b**).

Hydrogen bonding is an important aspect of the intermolecular interactions leading to the ordered morphology observed in the cyclized YY nanotubes. Proton NMR of the cyclized YY nanotubes and linear YY peptide in DMSO- $d_6$  indicate that the linear YY peptides (**SI Figure S5**) had amide proton peak at  $8.1$

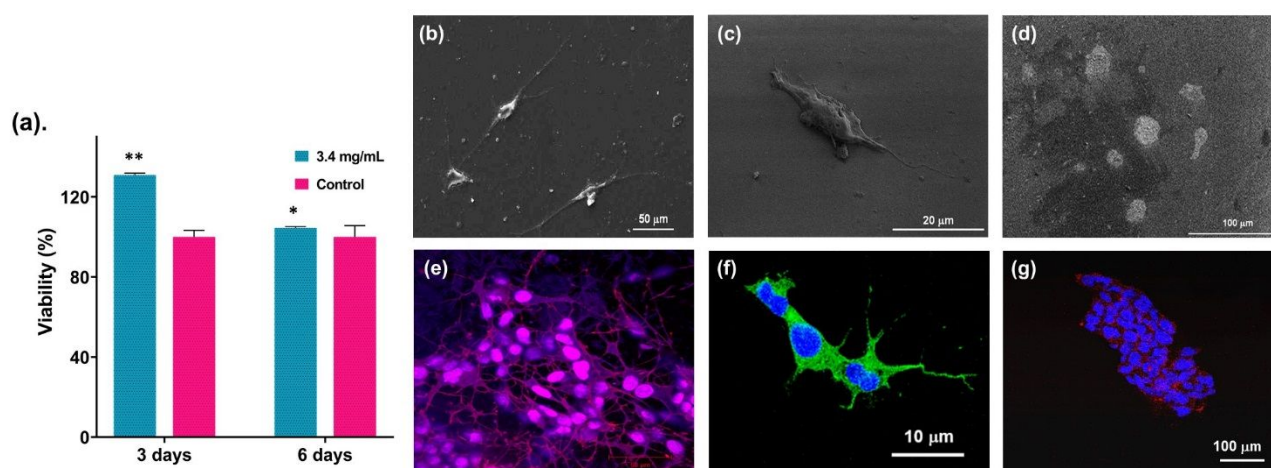


**Figure 6.** (a). Cell metabolic activity and viability assay (MTT) for SH-SY5Y cells grown on the cyclized YY nanotubes scaffold at 3- and 6 days post-seeding (\*\*  $P < 0.01$  and \*  $P < 0.1$ ,  $n=3$ ) (b). SEM image of SH-SY5Y cells cultured on the cyclized YY nanotubes substrates; (c). SEM image of single SH-SY5Y cell on cyclized YY nanotubes; (d). SEM image of control SH-SY5Y cells on glass coverslips (e). Confocal imaging of SH-SY5Y cells on cyclized YY nanotubes stained with phalloidin-rhodamine and counterstained with DAPI (f). Confocal imaging of SH-SY5Y cell on cyclized YY nanotubes stained with  $\beta$ -III tubulin; (g). Confocal imaging of control SH-SY5Y cells stained with phalloidin-rhodamine and counterstained with DAPI.

ppm, aromatic proton peaks in the range of  $6.6 - 7.0$  ppm, methylene peaks at  $4.2$  &  $4$  ppm and benzylic proton peaks at  $2.9$ ,  $3.2$  and  $3.7$  ppm respectively whereas the cyclized YY nanotubes (**SI Figure S5**) had a phenolic hydroxy peak at  $9.0$  ppm, amide proton peak at  $7.6$  ppm, aromatic proton peaks in the range of  $6.6 - 6.8$  ppm, symmetric methylene peaks at  $3.78$  ppm, and benzylic peaks at  $3.25$  ppm. Comparison of the NMR peaks in linear YY and cyclized YY nanotubes indicate an upfield shift of  $0.6$  ppm in the amide protons, and an upfield of  $\sim 0.2$  ppm in the aromatic, methylene, and benzylic protons. The  $^{13}\text{C}$  NMR of the cyclized YY nanotubes revealed the presence of amide carbon signal at  $166.73$  ppm and the phenolic hydroxy attached carbon peaks at  $156.54$ . The aromatic phenyl ring carbon peaks were at  $131.22$ ,  $127.02$ , and  $115.50$  ppm. In addition, benzylic carbons and chiral carbon appeared at  $39.27$  and  $56.21$  ppm, respectively. The chemical structure of cyclic YY

nanotubes was confirmed based on the  $^1\text{H}$  and  $^{13}\text{C}$  NMR spectra. Intermolecular hydrogen bonding in cyclized YY nanotubes was monitored using temperature-dependent NMR spectroscopy at temperatures ranging between  $298\text{ K--}313\text{ K}$  (**Figure 4a**). Upon temperature increase, amide (Hb) and hydroxyl (Ha) protons show an upfield shift. The overall shift was found to be  $0.07$  ppm ( $\delta 9.13$  to  $\delta 9.06$ ) for hydroxyl protons and  $0.10$  ppm ( $\delta 7.70$  to  $\delta 7.60$ ) for amide protons. The formation of hydrogen bonding leads to deshielding and proton shifts to a higher frequency (downfield). Therefore, the upfield shift with increasing temperature observed during the heating of the cyclized YY nanotubes can be attributed to the weakening of intermolecular hydrogen bonding between dipeptide monomers. The above changes in chemical shifts of amide and hydroxyl protons confirm their role in self-assembly via H-bonding.<sup>57</sup>

XRD patterns of lyophilized linear and cyclized YY nanotubes display several sharp reflection peaks indicating the highly crystalline nature of the self-assembled nanotubes (Figure 4b).

The cyclized nanotube samples show a complex XRD pattern indicative of high crystallinity which also differs from the linear YY nanotubes.<sup>58</sup> Though the indexing of the thermally-modified nanotube was not performed, the most likely unit cell is orthorhombic based on prior studies and observations.<sup>59, 60</sup> Both the linear and cyclized YY nanotubes demonstrate a high stiffness (loading moduli) in the range of 800-850 MPa as tested using the nanoindenter XP whereas Young's modulus was in the range of ~1.3 GPa which is in the range of self-assembled fibrils of  $\alpha$ -synuclein, A $\beta$  (1–42), and Tau, (2 – 4 GPa).<sup>61</sup> These nanotubes exhibit high Young's moduli due to the hydrogen bonding in the peptide backbone. In prior studies using primary neural cells and mesenchymal stem cells, proliferation and differentiation was influenced by the increase in Young's modulus.<sup>62, 63</sup>

Neural cells are sensitive to the topography of their microenvironment and in order to understand the cell-substrate interactions, PC-12 and SH-SY5Y cells were seeded on the YY nanotubes scaffold.<sup>64</sup> Cell survival and proliferation on the cyclized YY nanotubes scaffold were studied in both the cell lines, (PC12 and SH-SY5Y) using MTT analysis (Figure 5a & 6a). The average MTT values for the PC12 cells grown on cyclized YY nanotubes of 2 and 4 mg/mL concentrations, were recorded on 3 and 5 days. The increase in absorbance observed in MTT reduction assay with the number of days in culture, indicates cellular viability on the nanotube surface. Both concentrations of YY nanotubes demonstrated good cell viability and proliferation, in comparison with the control (untreated glass coverslip). Whereas, the lower concentration of cyclized YY nanotubes (2 mg/mL) demonstrate higher cell proliferation (~20% higher) compared to the control sample grown on untreated coverslips on days 3 and 5 as shown in Figure 5a. The P value was calculated using a regression analysis between

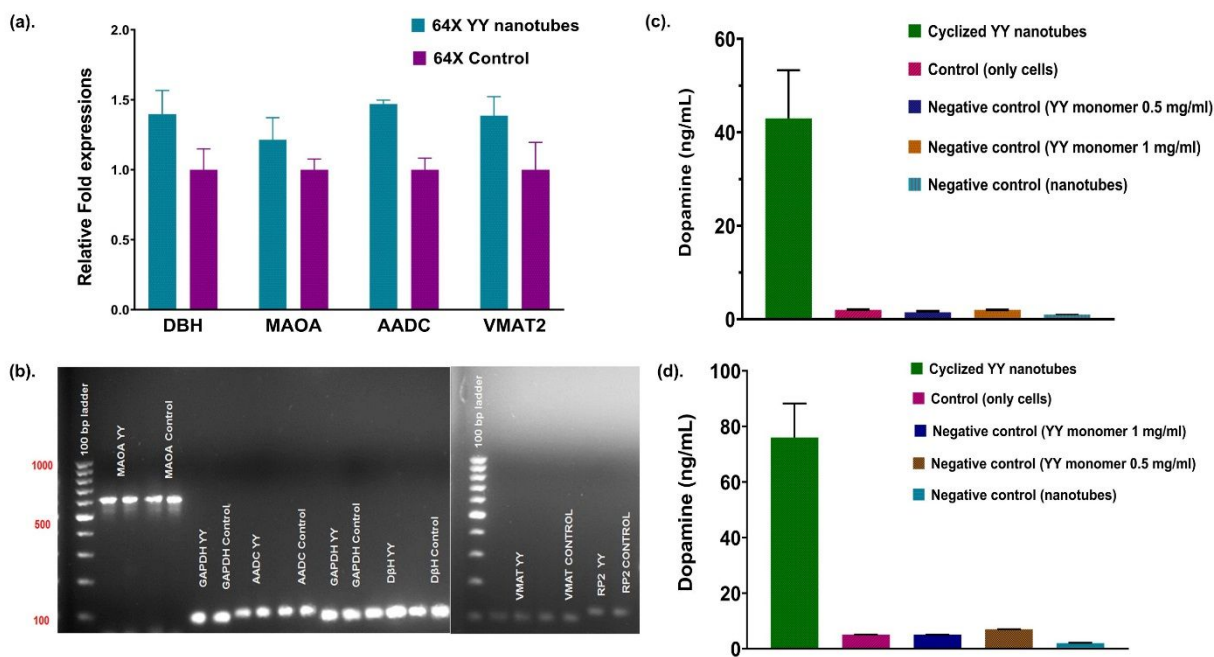


**Figure 7.** (a). Relative MAOA, AADC, VMAT-2, and  $D\beta H$  gene expression in SH-SY5Y cells after 8 days of culture on cyclized YY nanotubes. Samples normalized to GAPDH housekeeping gene (MAOA, AADC and  $D\beta H$ ) and RPII housekeeping gene (VMAT-2). (b). qPCR products of markers for DA release (64X, 4X concentrations): VMAT (105 bp),  $D\beta H$  (108 bp), MAOA (631 bp), AADC (120 bp) and housekeeping genes, RP2 (122 bp), GAPDH (106 bp); (c). DA release ELISA assay in PC12 cells after 8 days of culture on cyclized YY nanotubes scaffold; (d). DA release ELISA assay in SH-SY5Y cells after 8 days of culture on cyclized YY nanotubes scaffold.

average values measured in the two different concentration compared with the control. A 95% confidence interval was used

for the study, and at  $P < 0.005$  on day 3 and  $P < 0.05$  on day 5, the samples did not have any cytotoxic effects on the PC12 cells. In the case of the SH-SY5Y cells, a scaffold of cyclized YY nanotubes at 3.4 mg/mL concentration was used to test for

cytotoxicity effects on days 3 and 6, respectively and no significant difference in cytotoxicity was observed in comparison with the control. A 95% confidence interval was used for the study, and at  $P < 0.01$  on day 3 and  $P < 0.1$  on day 6, the samples did not have any cytotoxic effects on the SH-SY5Y cells. These results imply that the nanotubes were not cytotoxic to both PC12 and SH-SY5Y cells. The changes in cell morphology of PC12 and SH-SY5Y cells were observed using scanning electron microscopy (**Figures 5 b-c and 6 b-d**). Cells on the nanotubular substrate proliferated and were elongated due to the topography and stiffness of the nanotubes whereas the control coverslips had a higher percentage of round cells. The cells developed neural growth cones and neurite outgrowths on cyclized YY nanotubes scaffolds following 5 days of culture (**Figures 5b and 6b-c**). Confocal microscopy of cells stained with the cytoskeletal stain, phalloidin rhodamine, and counterstained with DAPI for the nucleus (**Figures 5d-e and 6e & 6g**) also confirmed the findings from the SEM imaging. SH-SY5Y cells were immunostained using a differentiation biomarker,  $\beta$ -III tubulin (green). The SH-SY5Y cells stained green

on nanotubes scaffold (positive, green), indicated the presence of the differentiation biomarker whereas the cells on a glass coverslip had no  $\beta$ -III tubulin (negative) (**Figure 6f**).

The dopaminergic and differentiation activity in SH-SY5Y and PC12 cells were monitored using changes in gene expression following their growth on cyclized YY nanotube scaffolds. The control samples for all experiments were neural cells grown on glass coverslips whereas the YY bands represent the cells exposed to cyclized YY nanotubes. Four genes pertaining to SH-SY5Y cells and two in the case of PC12 cells were investigated for DA metabolism, DA transportation, and differentiation of the cells.<sup>29, 65</sup> By analyzing total RNA extracted from the samples, expression of the different DA and differentiation gene segments was studied. A series of conventional and gradient PCR methods were used to optimize the primers' temperatures for qPCR analysis. The qPCR results were validated using the  $2^{-\Delta\Delta Ct}$  method (**Figure 7a**).<sup>46</sup> The respective qPCR products were observed on a 2.5% agarose gel to verify the amplification (**Figure 7b**). The SH-SY5Y cells expressed all genes encoding enzymes and molecules required for the synthesis of DA, in the absence of chemical differentiators such as retinoic acid. The cyclized YY nanotubes scaffold induced significant changes in D $\beta$ H, MAOA, VMAT-2 and AADC genes in SH-SY5Y cells, and COMT and  $\beta$  III-tubulin in PC12 cells, respectively as observed in the qPCR analysis (**SI Figure S6**). VMAT-2 and AADC are genes with a central role in DA synthesis and transportation in SH-SY5Y cells, and changes in their expression was confirmed by the qPCR analysis. ~40% fold changes in the expression of D $\beta$ H, VMAT-2 and AADC were observed in the case of SH-SY5Y cells cultured on cyclized YY nanotubes for 8 days. These results indicate that DA synthesis and storage inside vesicles may be upregulated in the presence of the cyclized YY nanotubes. However, expression levels of DAT and COMT expression were not observed to be elevated in the SH-SY5Y cells. A 20% increase in the dopamine breakdown enzyme, MAOA was also observed but was not correlated with an increase in protein expression, which needs to be studied further. MAOs on the surface of the

mitochondria are a secondary source of reactive oxygen species (ROS) but overexpression of ROS was not observed in the SH-SY5Y cells. The PC12 cells showed a 0.6%-fold change in the expression of COMT mRNA but a remarkably high change with respect to  $\beta$  III-tubulin with a ~22-fold increase (**SI Figure 7**). This signifies that the marker associated with differentiation of the neural cells was upregulated and differentiation was highly likely during the growth of the cells on the cyclized YY nanotubes scaffold (**Figure 7a**). The observed increase in the differential gene expression of COMT and MAOA in PC12 and SH-SY5Y cells respectively, as compared to control samples, indicates that there is higher DA release or the conversion of DA into metabolites occurs at higher levels as compared to the levels in control samples.

In parallel, the release of intra- and intercellular DA in PC12 and SH-SY5Y cells after 8 days on the cyclized YY nanotubes scaffold was analyzed using ELISA (**Figure 7c & 7d**).<sup>66, 67</sup> The overall release of DA from PC12 cells cultured on the cyclized YY nanotubes scaffold was 43 ng/mL in comparison to control scaffold of glass coverslips where DA released was 2 ng/mL (**Figure 7c**). Negative control with addition of YY monomer, also had DA release of 1-2 ng/mL based on concentration of monomer added into the cell culture media. The ELISA kit was not sensitive to the YY nanotubes or monomer as demonstrated by the negative control with DA released at 0.8 ng/mL. Similarly, SH-SY5Y cells show an increase of ~70 ng/mL with respect to the control. Negative control with addition of YY monomer, also had DA release of 5-7 ng/mL based on concentration of monomer added into the cell culture media (**Figure 7d**). The fractional (DA release per cell) DA release was 0.13 pg/mL and 0.23 pg/mL for PC12 and SH-SY5Y cells cultured on the cyclized YY nanotubes scaffold respectively, as opposed to the control values (glass coverslips) of .0016 pg/mL and .016 pg/mL for PC12 and SH-SY5Y cells respectively. D $\beta$ H plays a significant role in the transformation of the synthesized DA into noradrenaline and the higher levels of D $\beta$ H observed in the QPCR results indicate that higher levels of transformation should be occurring the SH-SY5Y cells. But despite this, we have observed higher amounts of DA synthesized in agreement with previous studies.<sup>29, 68</sup> The presence of free tyrosine may influence the dopaminergic gene expression and DA expression in the PC12 and SH-SY5Y cells. At the end of 3 days, 50  $\mu$ L of the cell culture media was tested for the presence of free tyrosine in solution and the measured tyrosine concentration was 100  $\mu$ M using a standard curve (**SI Figure 8**). The tyrosine assay kit was sensitive to tyrosine, YY as well as DA, so this assay was inconclusive in determining the presence of free tyrosine in the cell culture media.

## D. Conclusions

Design and synthesis of biomaterials that support the regeneration of cells while mimicking the characteristics of cellular environments and providing physicochemical cues, is a field which has garnered attention in the past decade. In this study, we have explored the synthesis of cyclized YY nanotubes, and their application as scaffolds for neural cells. We have addressed some of the issues associated with the stability of linear peptide nanostructures, by the heat-induced cyclization

to produce physiologically stable nanotube scaffolds. This is a reliable and quick process, which could reduce the complexity associated with the synthesis of cyclic peptides and the removal of the solvents. The computational modeling sheds light on the interactions and arrangements of the peptide assemblies. The most stable conformer, the cyclic YY monomer has additional hydrogen bonding and a diketopiperazine ring contributing to the stability. The dipeptide dimers and hexamers favor configurations which maximizes hydrogen bonding and  $\pi$ - $\pi$  stacking. The chemical, physical characterization of the cyclized nanotubes are complementary to the simulation studies and prove that thermal cyclization did not affect the nanotube aspect ratios, the chemical properties and improved physiological stability, also discussed in our previous study. Neural cells are responsive to micron and nanoscale topographic features, which provide cues for cellular proliferation and attachment.<sup>31, 32</sup> Cytotoxicity studies indicate that the YY nanotubes promote proliferation of neural cells and their structure contributes to the cellular attachment while promoting the formation of growth cones and neurite outgrowths. The morphology of the cells and the nuclear distortion consequently modify gene expression, affecting the fate and behavior of the cells. The self-assembled YY peptide-based nanotubes provides a biodegradable scaffold which supports neural cell growth, promotes DA expression and differentiation in neural cells. While toxicity studies indicate biocompatibility and cellular studies show biological activity of the nanotubes in cellular attachment, proliferation, and differentiation, long-term animal studies are required for their application in human neural regeneration.

### Conflicts of interest

There are no conflicts to declare.

### Acknowledgements

The electron microscopy images in this work were obtained using a scanning electron microscope supported by the National Science Foundation under Grant No. 1726239. We acknowledge the support by the University of Massachusetts Dartmouth Provost's office for the multi-disciplinary seed funding. We are grateful to the Materials and Manufacturing directorate of the Air Force Research Laboratory for allowing us access to the CD spectrometer and nanoindenter XP for materials characterization. We are grateful to Earl Ada of the Materials characterization Facility at University of Massachusetts at Lowell for help with the transmission electron microscopy. We are also grateful to the Department of geological sciences and Jessica Campbell at Bridgewater State University for the use of their XRD facility.

### References

- G. M. Whitesides, J. P. Mathias and C. T. Seto, *Science*, 1991, **254**, 1312-1319.
- S. Zhang, D. M. Marini, W. Hwang and S. Santoso, *Current opinion in chemical biology*, 2002, **6**, 865-871.
- S. Vauthey, S. Santoso, H. Gong, N. Watson and S. Zhang, *Proceedings of the National Academy of Sciences*, 2002, **99**, 5355-5360.
- D. DeVore and R. Gruebel, *Biochemical and biophysical research communications*, 1978, **80**, 993-999.
- K. Stewart, P. Spedding, M. Otterburn and D. Lewis, *Journal of applied polymer science*, 1997, **66**, 2365-2376.
- K. A. Tilley, R. E. Benjamin, K. E. Bagorogoza, B. M. Okot-Kotber, O. Prakash and H. Kwen, *Journal of Agricultural and Food Chemistry*, 2001, **49**, 2627-2632.
- W. Peelaerts and V. Baekelandt, *Nature structural & molecular biology*, 2016, **23**, 359-360.
- Z. Qin, D. Hu, S. Han, D. P. Hong and A. L. Fink, *Biochemistry*, 2007, **46**, 13322-13330.
- B. P. Partlow, M. B. Applegate, F. G. Omenetto and D. L. Kaplan, *ACS Biomaterials Science & Engineering*, 2016, **2**, 2108-2121.
- K.-I. Min, D.-H. Kim, H.-J. Lee, L. Lin and D.-P. Kim, *Angewandte Chemie International Edition*, 2018, **57**, 5630-5634.
- Y.-F. Huang, S.-C. Lu, Y.-C. Huang and J.-S. Jan, *Small*, 2014, **10**, 1939-1944.
- I. J. Rhile, T. F. Markle, H. Nagao, A. G. DiPasquale, O. P. Lam, M. A. Lockwood, K. Rotter and J. M. Mayer, *Journal of the American Chemical Society*, 2006, **128**, 6075-6088.
- J. J. Warren, J. R. Winkler and H. B. Gray, *FEBS letters*, 2012, **586**, 596-602.
- S.-Y. Tarn and R. H. Roth, *Biochemical Pharmacology*, 1997, **53**, 441-453.
- S. Yano, K. Moseley and C. Azen, *The Journal of pediatrics*, 2014, **165**, 184-189.e181.
- D. Shurtleff, J. R. Thomas, J. Schrot, K. Kowalski and R. Harford, *Pharmacology Biochemistry and Behavior*, 1994, **47**, 935-941.
- R. J. Wurtman, F. Hefti and E. Melamed, *Pharmacological Reviews*, 1980, **32**, 315-335.
- J. D. Milner and R. J. Wurtman, *Biochemical pharmacology*, 1986, **35**, 875-881.
- P. Macha, L. Perreault, Y. Hamedani, M. L. Mayes and M. C. Vasudev, *ACS Applied Bio Materials*, 2018, **1**, 1266-1275.
- G. Guroff, in *Cell Culture in the Neurosciences*, eds. J. E. Bottenstein and G. Sato, Springer US, Boston, MA, 1985, DOI: 10.1007/978-1-4613-2473-7\_8, pp. 245-272.
- J. Wang, M. F. Rahman, H. M. Duhart, G. D. Newport, T. A. Patterson, R. C. Murdock, S. M. Hussain, J. J. Schlager and S. F. Ali, *Neurotoxicology*, 2009, **30**, 926-933.
- H.-r. Xie, L.-s. Hu and G.-y. Li, *Chinese medical journal*, 2010, **123**, 1086-1092.
- H. Xicoy, B. Wieringa and G. J. M. Martens, *Molecular Neurodegeneration*, 2017, **12**, 10.
- L. A. Greene and J. C. McGuire, *Nature*, 1978, **276**, 191-194.
- Z. Lyu, X. Shi, J. Lei, Y. Yuan, L. Yuan, Q. Yu and H. Chen, *Journal of Materials Chemistry B*, 2017, **5**, 1896-1900.
- G. F. G. Allen, Y. Ullah, I. P. Hargreaves, J. M. Land and S. J. R. Heales, *Neurochemistry International*, 2013, **62**, 684-694.
- L. Yavich, M. M. Forsberg, M. Karayiorgou, J. A. Gogos and P. T. Männistö, *The Journal of Neuroscience*, 2007, **27**, 10196-10209.

28. M. Naoi and W. Maruyama, *Expert Review of Neurotherapeutics*, 2009, **9**, 1233-1250.
29. R. Filograna, L. Civiero, V. Ferrari, G. Codolo, E. Greggio, L. Bubacco, M. Beltramini and M. Bisaglia, *PLOS ONE*, 2015, **10**, e0136769.
30. T. N. Taylor, W. M. Caudle and G. W. Miller, *Parkinson's Disease*, 2011, **2011**, 124165.
31. F. Haq, V. Anandan, C. Keith and G. Zhang, *International journal of nanomedicine*, 2007, **2**, 107.
32. M.-H. Kim, M. Park, K. Kang and I. S. Choi, *Biomaterials Science*, 2014, **2**, 148-155.
33. Y. Zhao, N. E. Schultz and D. G. Truhlar, *The Journal of Chemical Physics*, 2005, **123**, 161103.
34. P. C. P. Hariharan, J. A. , *Theor. Chim. Acta*, 1973, **28** 213-222.
35. M. W. Schmidt, K. Baldrige, J. Boatz, S. Elbert, M. S. Gordon, J. H. Jenson, S. Koseki, N. Matsunaga, K. A. Nguyen, S. J. Su, T. L. Windus, M. Dupuis and J. Montgomery, *J. Comp. Chem.*, 1993, **14**, 1347-1363.
36. S. Grimme, J. Antony, S. Ehrlich and H. Krieg, *The Journal of Chemical Physics*, 2010, **132**, 154104.
37. M. Gaus, Q. Cui and M. Elstner, *Journal of Chemical Theory and Computation*, 2011, **7**, 931-948.
38. M. Gaus, A. Goez and M. Elstner, *Journal of Chemical Theory and Computation*, 2013, **9**, 338-354.
39. K. Kitaura, E. Ikeo, T. Asada, T. Nakano and M. Uebayasi, *Chemical Physics Letters*, 1999, **313**, 701-706.
40. J. E. D. Glendenning, K. Badenhop, A. E. Reed, J. E. Carpenter, J. A. Bohmann, C. M. Morales, P. Karafiloglou, C. R. Landis, and F. Weinhold, 2018.
41. A. V. Marenich, C. J. Cramer and D. G. Truhlar, *The journal of physical chemistry. B*, 2009, **113**, 6378-6396.
42. F. Neese, *Wiley Interdisciplinary Reviews: Computational Molecular Science*, 2012, **2**, 73-78.
43. J. Kovalevich and D. Langford, *Methods Mol Biol*, 2013, **1078**, 9-21.
44. D. Gerlier and N. Thomasset, *Journal of immunological methods*, 1986, **94**, 57-63.
45. L. Agholme, T. Lindström, K. Kågedal, J. Marcusson and M. Hallbeck, *Journal of Alzheimer's disease : JAD*, 2010, **20**, 1069-1082.
46. K. J. Livak and T. D. Schmittgen, *Methods*, 2001, **25**, 402-408.
47. P. Wang, A. Xiong, Z. Gao, X. Yu, M. Li, Y. Hou, C. Sun and S. Qu, *PloS one*, 2016, **11**, e0160885-e0160885.
48. C. Liu, L. Kershberg, J. Wang, S. Schneeberger and P. S. Kaeser, *Cell*, 2018, **172**, 706-718.e715.
49. G. Park, Y.-S. Jung, M.-K. Park, C. H. Yang and Y.-u. Kim, *Scientific Reports*, 2018, **8**, 14981.
50. M. Mayes and L. Perreault, *Computational and Theoretical Chemistry*, 2018, **1131**, 99-109.
51. J. Kong and S. Yu, *Acta biochimica et biophysica Sinica*, 2007, **39**, 549-559.
52. J. T. Pelton and L. R. McLean, *Analytical biochemistry*, 2000, **277**, 167-176.
53. F. Zhu, N. W. Isaacs, L. Hecht and L. D. Barron, *Structure*, 2005, **13**, 1409-1419.
54. M. Tsuboi, Y. Ezaki, M. Aida, M. Suzuki, A. Yimit, K. Ushizawa and T. Ueda, *Biospectroscopy*, 1998, **4**, 61-71.
55. T. Kamiyama, T. Miura and H. Takeuchi, *Biophysical chemistry*, 2013, **173-174C**, 8-14.
56. B. Peter, A. Polyansky, S. Fanucchi and H. Dirr, *Biochemistry*, 2013, **53**, 57-67.
57. J. R. Cochrane, J. M. White, U. Wille and C. A. Hutton, *Organic Letters*, 2012, **14**, 2402-2405.
58. N. Amdursky, P. Beker, I. Koren, B. Bank-Srouer, E. Mishina, S. Semin, T. Rasing, Y. Rosenberg, Z. Barkay, E. Gazit and G. Rosenman, *Biomacromolecules*, 2011, **12**, 1349-1354.
59. R. Degeilh and R. Marsh, *Acta Crystallographica*, 1959, **12**, 1007-1014.
60. C. H. Görbitz, *Chemistry – A European Journal*, 2001, **7**, 5153-5159.
61. J. Adamcik, C. Lara, I. Usov, J. S. Jeong, F. S. Ruggeri, G. Dietler, H. A. Lashuel, I. W. Hamley and R. Mezzenga, *Nanoscale*, 2012, **4**, 4426-4429.
62. M. L. Previtera, C. G. Langhammer and B. L. Firestein, *Journal of Bioscience and Bioengineering*, 2010, **110**, 459-470.
63. S. Ali, I. B. Wall, C. Mason, A. E. Pelling and F. S. Veraitch, *Acta Biomaterialia*, 2015, **25**, 253-267.
64. J. M. Stukel and R. K. Willits, *Tissue Eng Part B Rev*, 2016, **22**, 173-182.
65. M. R. Ostadali, G. Ahangari, M. B. Eslami, A. Razavi, M. R. Zarrindast, H. R. Ahmadkhaniha and J. Boulhari, *Iran J Allergy Asthma Immunol*, 2004, **3**, 169-174.
66. X. Gu, L. Liu, Q. Shen and D. Xing, *Cellular Signalling*, 2017, **37**, 103-114.
67. J.-H. Chang, P.-H. Tsai, W. Chen, S.-H. Chiou and C.-Y. Mou, *Journal of Materials Chemistry B*, 2017, **5**, 3012-3023.
68. J. L. Biedler, S. Roffler-Tarlov, M. Schachner and L. S. Freedman, *Cancer research*, 1978, **38**, 3751-3757.

